Journal of the Ceramic Society of Japan 131 [4] 57-61 2023
DOI https://doi.org/10.2109/jcersj2.22167

JCS-Japan

FULL PAPER

Neodymium(III)-doped $Y_3Al_2Ga_3O_{12}$ garnet for multipurpose ratiometric thermometry: From cryogenic to high temperature sensing

Michele Back[1,2,†], Jian Xu[2,3], Jumpei Ueda[2,4] and Setsuhisa Tanabe[2]

[1] Department of Molecular Sciences and Nanosystems, Ca' Foscari University of Venice, Via Torino 155, 30170, Mestre, Italy
[2] Graduate School of Human and Environmental Studies, Kyoto University, Kyoto 606–8501, Japan
[3] International Center for Young Scientists (ICYS), National Institute for Materials Science (NIMS), Tsukuba, Ibaraki 305–0044, Japan
[4] Materials Chemistry Frontiers, Japan Advanced Institute of Science and Technology (JAIST), 1–1 Asahidai, Nomi, Ishikawa 923–1292, Japan

Nd^{3+}-doped $Y_3Al_2Ga_3O_{12}$ garnet ceramic pellet was prepared by solid state reaction and used as prototype to investigate the potential of Nd^{3+}-activated garnet phosphors as Boltzmann thermometers for cryogenic and high temperature ranges. Despite the conventional use of the near-infrared emitting Nd^{3+}-activated phosphors for biological applications, their real use is hindered by a low sensitivity in the physiological temperature range. Instead, the photoluminescence analysis in the 100–800 K range demonstrated interesting performances in both the cryogenic and high temperature ranges. Indeed, by taking advantage of the Stark levels of $^4F_{3/2}$ (Z-levels) and the ratio between the emission from the $^4F_{5/2}$ and the $^4F_{3/2}$ excited states is possible to build two reliable Boltzmann thermometers in the same material working in the cryogenic temperature range (100–220 K) and at high temperatures (300–800 K), respectively.

Key-words : YAGG, Ratiometric thermometry, Luminescence, Garnet, Boltzmann distribution, Neodymium

[Received December 29, 2022; Accepted January 15, 2023]

1. Introduction

In the last decade, the use of luminescent materials as ratiometric thermometers based on the ratio between the emissions from two excited states has been extensively investigated.[1)–4)] Despite the wide variety of thermometers proposed, the use of the luminescent signals originated from two thermally coupled excited states of the same luminescent center, the so-called Boltzmann thermometers, is still recognized among the most reliable systems. In this view, the most popular thermometers are based on Er^{3+},[5)] Nd^{3+},[6)–10)] Tm^{3+} [11),12)] but also Cr^{3+} [13)–15)] ions.

Since the electronic structure of Nd^{3+} allows to work in the biological windows by both the excitation and emission, Nd^{3+}-activated phosphors are commonly investigated as optical thermometers for biological applications.[16)–19)] Even though the energy gap of about 900–1000 cm^{-1} between the $^4F_{3/2}$ and $^4F_{5/2}$ energy levels seems to be quite promising, the large difference in the intensity between the transitions starting from these two excited states results in a large uncertainty at room temperature. On the other hand, when the two Stark levels of the $^4F_{3/2}$ state (Z_1 and Z_2) are employed to build a thermometric parameter, the energy gaps between the excited states are typically of few tens to about a hundred cm^{-1}, leading, in the physiological temperature range, to small values of sensitivity.

Luminescent thermometers find interesting applications in many other technological fields such as catalysis,[13),20),21)] microfluidic[22)] and microelectronics,[23)] to name a few, making the development of reliable optical thermometers characterized by high sensitivities at both cryogenic and high temperatures still a challenge.

By using Nd^{3+}-doped $Y_3Al_2Ga_3O_{12}$ garnet as prototype, we investigate the potential of this family of materials as Boltzmann thermometers. Even though the materials are typically proposed for biological applications, herein we demonstrate interesting performances in the cryogenic and high temperature ranges.

2. Experimental procedure

YAGG:Nd^{3+} ceramic phosphor with the compositions of $Y_{2.94}Nd_{0.06}Al_2Ga_3O_{12}$ was fabricated by a conventional solid-state reaction method. Y_2O_3 (99.99 %), Al_2O_3 (99.99 %), Ga_2O_3 (99.99 %) and Nd_2O_3 (99.99 %) were used as raw materials. The starting powder was mixed by a ball milling method (Premium Line P-7, Fritsch Co. Ltd.) with anhydrous alcohol for several hours. The mixed powder was dried at 80 °C for 36 h, compacted to form a ceramic green body (ϕ20 mm, 2 mm thickness) under uni-

† Corresponding author: M. Back; E-mail: michele.back@unive.it

axial pressing of 50 MPa, and finally sintered at 1600 °C for 10 h in air.

X-ray powder diffraction (XRPD) measurements were performed using a diffractometer (XRD6000, Shimadzu) with Cu Kα radiation ($\lambda = 1.54056$ Å). The diffuse reflectance spectra were measured by a spectrophotometer (UV3600, Shimadzu) equipped with an integrating sphere. Barium sulfate is used as a standard for calibration. Photoluminescence excitation (PLE) spectra were measured by an InGaAs photodiode (IGA-030-H, Electro-Optical System Inc.) coupled with a short-cut (990 nm) and a long-cut (1300 nm) filter, a monochromator (SpectraPro-300i, Acton Research Corporation) and a 100 W halogen lamp (MHAA-100W, Moritex Corporation) as excitation source. Photoluminescence (PL) measurements were performed with the use of a USB-powered LED mount (LEDMT1F, Thorlabs) with a 590 nm LED (full width half maximum = 16 nm), equipped with a collimator, and collecting with a Si CCD spectrometer (QE-65Pro, Ocean Optics) coupled with a fiber. The temperature dependent PL spectra were collected with a temperature-controlled stage (10 035 L, Linkam). All of the spectra were calibrated by means of a standard halogen lamp (DH-2000CAL, Ocean Optics) to obtain spectra in the photon flux scale.

3. Results and discussion

Aluminium and gallium-based $A_3(Al,Ga)_5O_{12}$ garnets are among the most interesting families of host compounds in the optical field,[24] finding applications as phosphors (the most famous YAG:Ce^{3+}), persistent luminescent materials[25] and lasers (YAG:Nd^{3+} [26]) characterized by high quantum yields. Indeed, the structure allows to accommodate a wide variety of luminescent ions such as lanthanide ions in the dodecahedral sites and transition metal ions in both octahedral and tetrahedral sites [**Fig. 1**(a)].

As prototype to investigate the potential of Nd^{3+}-doped garnets as optical thermometers for different temperature regimes, the garnet compound $Y_3Al_2Ga_3O_{12}$ (YAGG) was selected. The XRPD pattern confirmed the stabilization of the cubic $Ia\bar{3}d$ single phase [Fig. 1(b)] in which Nd^{3+} substitutes Y^{3+} in the dodecahedral site.

Figure 1(c) shows the Kubelka–Munk function calculated by the reflectance spectrum and the PL emission and excitation spectra of YAGG:Nd^{3+} in the range matching with the highly efficient commercial Si-detectors. In this spectral range, the emission is mainly characterized by the $^4F_{3/2} \rightarrow {}^4I_{9/2}$ transition falling into the first biological window. In addition, the PLE spectrum is composed by a series of absorption lines due to the f-f transitions of Nd^{3+} ion allowing the excitation in the whole visible range, an appealing feature from the application point of view.

To access the potential of the system as luminescent thermometer, the temperature dependence of the PL spectra was investigated in the 100–800 K range [**Fig. 2**(a)]. By increasing the temperature, the emission at about 810 nm due to the $^4F_{5/2} \rightarrow {}^4I_{9/2}$ transition (I_5) clearly increases with respect to the emission at about 880 nm due to the $^4F_{3/2} \rightarrow {}^4I_{9/2}$ transition (I_3) because of the relative population of the higher lying $^4F_{5/2}$ excited states with respect to $^4F_{3/2}$ [scheme in Fig. 2(b)]. Indeed, the luminescence intensity ratio of the two transitions used as thermometric parameter should follows a Boltzmann law:

$$LIR_{53} = I_5/I_3 = B_{53}\exp\left(-\frac{\Delta E_{53}}{k_B T}\right)$$

where ΔE_{53} is the energy gap between the $^4F_{5/2}$ and $^4F_{3/2}$ excited states, k_B is the Boltzmann constant and $B_{53} = g_5A_5N_5/g_3A_3N_3$ with g_i, A_i and N_i the degeneracy of the emitting level i, the spontaneous emitting rate and the population of the excited state, respectively.

By plotting the logarithm of the intensity ratio between the two excited states as a function of the inverse of the temperature, $\ln(I_5/I_3)$ versus T^{-1}, it is possible to determine (i) the energy gap ΔE_{53} between the excited states and (ii) the temperature range in which the Boltzmann law is working. The ΔE_{53} of 879 cm^{-1} estimated is in agreement with the energy gap estimated from the baricenters of the spectral bands (about 1000 cm^{-1}). In addition, the Boltzmann plot shows a good linearity starting from about 300 K with a clear deviation for lower temperatures.

Even though the energy difference between the $^4F_{5/2}$ and $^4F_{3/2}$ excited states looks particularly suitable for the

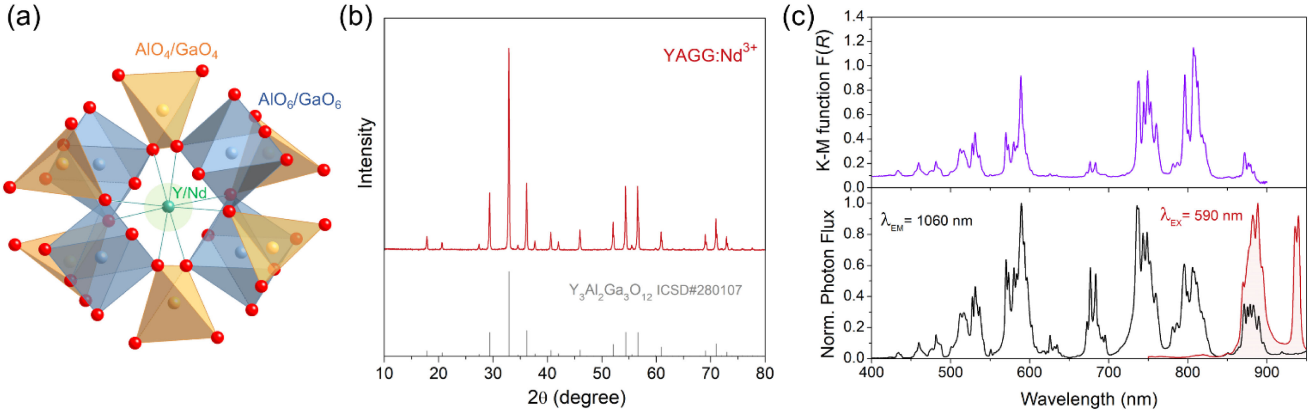

Fig. 1. (a) Schematic structure of the garnet structure, (b) XRPD pattern and (c) Kubelka–Munk function, PL and PLE spectra of YAGG:Nd^{3+} exciting at 590 nm and collecting at 1060 nm, respectively.

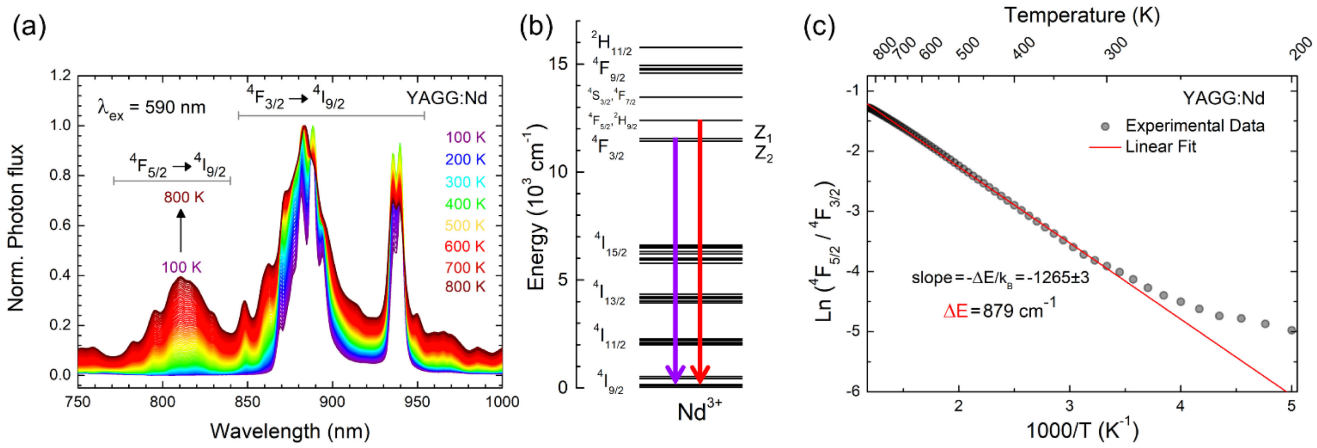

Fig. 2. (a) Temperature dependence of the PL spectra of YAGG:Nd^{3+} in the 80–800 K temperature range under excitation at 590 nm. The spectra are normalized to the $^4F_{3/2} \rightarrow {}^4I_{9/2}$ emission. (b) Energy level diagram of the Nd^{3+} ion in YAGG. Arrows highlight the transitions considered in this work ($^4F_{3/2} \rightarrow {}^4I_{9/2}$, $^4F_{5/2} \rightarrow {}^4I_{9/2}$, and $Z_{1,2} \rightarrow R_5$). (c) Plots of $\ln(I_5/I_3)$ versus T^{-1} to calibrate the thermometer using the $^4F_{5/2}$-$^4F_{3/2}$ couple. The red line represents the linear fit of the Boltzmann plot.

design of an optical thermometers with high performances for biological applications, the emission from the higher lying $^4F_{5/2}$ state is usually quite weak in the physiological temperature range resulting in unsuitable thermal resolutions. However, the thermal stability of the emission at high temperatures makes the system particularly interesting for high temperature sensing where the emissions from the higher lying $^4F_{5/2}$ state are relevant.

On the other hand, with the aim of developing thermometers for biological applications, a lot of interest was devoted to the use of the two Stark levels (Z_1 and Z_2) of the $^4F_{3/2}$ state. However, the narrow energy gap between these two levels can be exploited not only in the physiological temperature range but also at low temperature for cryothermometry. Indeed, the small energy gap value between the two states is particularly suitable to allow thermal populations also at low temperatures. The temperature dependent PL emission spectra collected in the 100–400 K range [**Fig. 3**(a)] show the relative increase of the emission from the higher lying Z_2 state with respect to Z_1 by increasing the temperature. In addition, the deconvolution of the spectrum [Fig. 3(b)] allows to estimate an energy gap between the excited states ΔE_{12} of 50 cm^{-1}.

By considering the ratio between the two transitions from Z_1 (I_1) and Z_2 (I_2) as a thermometric parameter:

$$LIR_{12} = I_2/I_1 = B_{21} \exp\left(-\frac{\Delta E_{12}}{k_B T}\right)$$

the Boltzmann plot in Fig. 3(c) evidences a clear deviation from the expected linearity.

The plot can be divided into two different regions and fit by two different linear curves in the temperature ranges of 100–220 and 220–400 K. The fit of the low temperature range allows to estimate an energy gap of 45 cm^{-1}, in very good agreement with the spectral estimation in Fig. 3(b), resulting particularly reliable as Boltzmann thermometer. Instead, the deviation from the linear trend characterized by the expected ΔE_{12} at temperatures higher than 220 K (characterized by an energy gap of 105 cm^{-1}) is not completely understood at the present and could be related to the involvement of phonons.

To discuss the thermometric performances of the thermometers, we considered the figure of merit described by the relative sensitivity S_r and the thermal resolution δT, defined as:

$$S_r = \frac{1}{LIR}\frac{\partial LIR}{\partial T}$$
$$\delta T = \frac{1}{S_r}\frac{\delta LIR}{LIR}$$

where δLIR is the uncertainty in the determination of LIR.

The plot of the S_r values of the two thermometric parameters calculated in the different ranges of linearity of the Boltzmann low [**Fig. 4**(a)] shows interesting values in both the cryogenic and high temperature ranges. On the other hand, the thermal resolution values in the cryogenic range by considering the Z_1-Z_2 couple are smaller than 1 K in the whole temperature range of linearity of the Boltzmann plot and the values of the thermometer based on the $^4F_{5/2}$-$^4F_{3/2}$ couple evidence an interesting situation in which values around 2 K can be achieved at high temperatures up to 800 K [Fig. 4(b)]. Such appealing values are due to the strong intensity of Nd^{3+} in the garnet structure giving high signal-to-noise values.

By considering the high reliability of the Boltzmann thermometers, the relative sensitivity of 0.45 % K^{-1} obtained at 100 K is quite promising, being comparable with the value reported for state-of-the-art cryogenic Boltzmann thermometers such as in the case of $CaHfO_3$:Cr^{3+} (0.3 % K^{-1} at 100 K[15]).

In addition, it is worth noting that from the application point of view, YAGG:Nd^{3+} is also characterized by an intrinsic high quantum yield and thermal stability already exploited for lasing applications, making the system particularly promising.

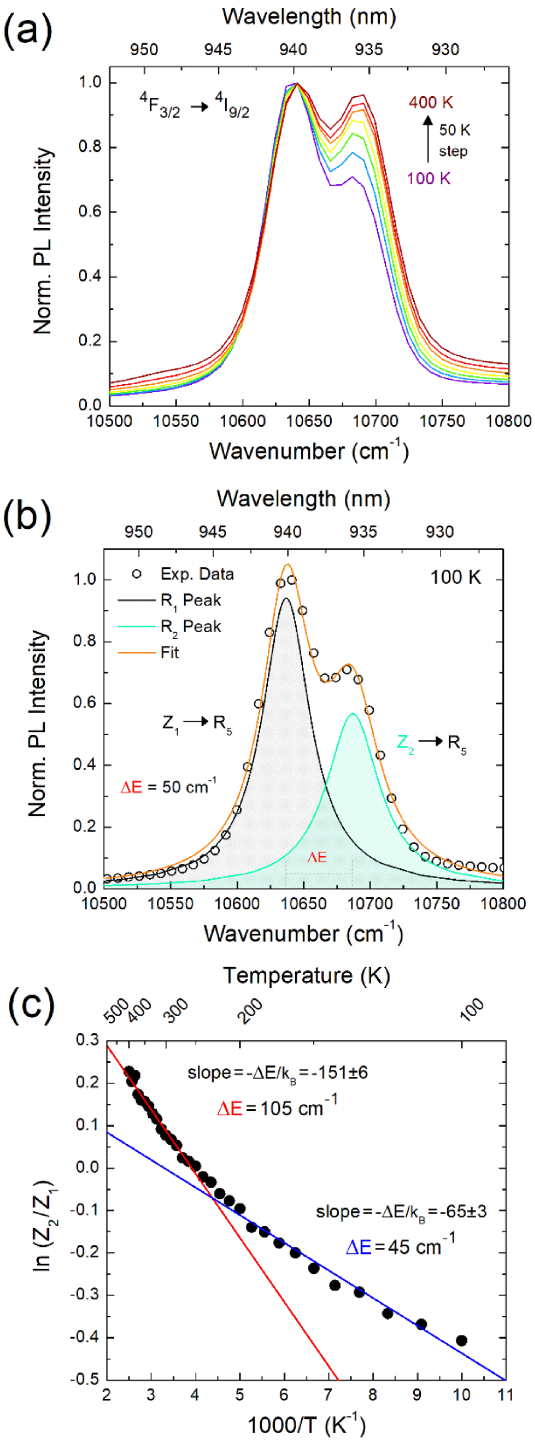

Fig. 3. (a) Temperature dependence of the PL spectra of YAGG:Nd^{3+} in the 100–400 K temperature range under excitation at 590 nm. The spectra are normalized to the Z_1 emission. (b) PL integrated area of the emission bands of $Z_{1,2} \rightarrow R_5$ transitions as a function of temperature. (c) Spectral deconvolution of the PL spectrum. (d) Plots of $\ln(I_2/I_1)$ versus T^{-1} to calibrate the thermometer using the Z_2-Z_1 couple. The blue line and red line represent the linear fits.

4. Conclusions

In summary, the potential of YAGG:Nd^{3+} system as luminescent thermal sensor is investigated in the 100–800 K temperature range. The possibility to design two reliable thermometric parameters based on the Boltzmann law in the same material is demonstrated. Furthermore, (i) the high temperature stability makes this system suitable for high temperature sensing by considering the thermal equilibrium between $^4F_{3/2}$ and $^4F_{5/2}$ excited states up to 800 K while (ii) for low temperatures from 100 to 220 K, the thermometer based on the Z_1-Z_2 couple is demonstrated to be a suitable and reliable cryogenic thermometer with thermal resolution lower than 1 K in the whole temperature range.

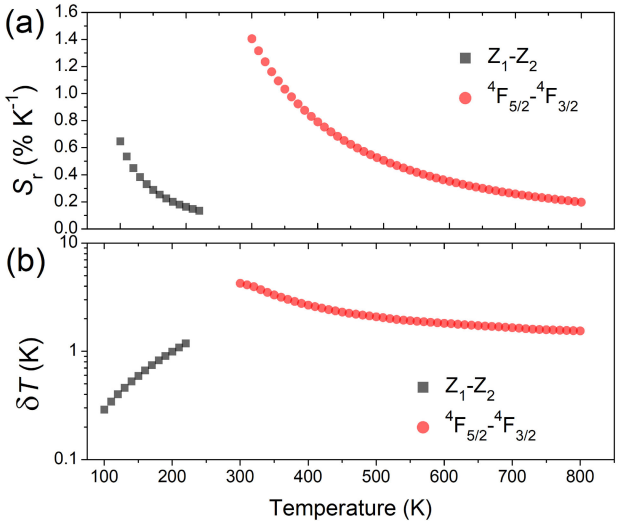

Fig. 4. Temperature dependence of the relative sensitivity (a) and thermal resolution (b) for the thermometers build by considering the ratio between the emissions of the $^4F_{5/2}$-$^4F_{3/2}$ couple and the Z_2-Z_1 couples.

Acknowledgments Work by M.B. was financially supported by the Grant-In-Aid for JSPS Fellows (17F17761).

References

1) C. D. Brites, S. Balabhadra and L. D. Carlos, *Adv. Opt. Mater.*, 7, 1801239 (2018).
2) M. D. Dramićanin, *J. Appl. Phys.*, 128, 040902 (2020).
3) E. J. McLaurin, L. R. Bradshaw and D. R. Gamelin, *Chem. Mater.*, 25, 1283–1292 (2013).
4) D. Jaque and F. Vetrone, *Nanoscale*, 4, 4301–4326 (2012).
5) F. Vetrone, R. Naccache, A. Zamarron, A. J. de la Fuente, F. Sanz-Rodriguez, L. Martinez Maestro, E. M. Rodriguez, D. Jaque, J. Garcia Sole and J. A. Capobianco, *ACS Nano*, 4, 3254–3258 (2010).
6) D. Wawrzynczyk, A. Bednarkiewicz, M. Nyk, W. Strek and M. Samoc, *Nanoscale*, 4, 6959–6961 (2012).
7) M. Back, J. Ueda, J. Xu, D. Murata, M. G. Brik and S. Tanabe, *ACS Appl. Mater. Inter.*, 11, 38937–38945 (2019).
8) M. Back, E. Casagrande, E. Trave, D. Cristofori, E. Ambrosi, F. Dallo, M. Roman, J. Ueda, J. Xu, S. Tanabe, A. Benedetti and P. Riello, *ACS Appl. Mater. Inter.*, 12, 55195–55204 (2020).
9) M. Suta, Z. Anric, V. Dordevic, S. Kuzman, M. D. Dramicanin and A. Meijerink, *Nanomaterials-Basel*, 10,

543 (2020).
10) M. Back, J. Xu, J. Ueda, A. Benedetti and S. Tanabe, *Chem. Mater.*, **34**, 8198–8206 (2022).
11) W. Xu, X. Gao, L. Zheng, Z. Zhang and W. Cao, *Sensor. Actuat. B-Chem.*, **173**, 250–253 (2012).
12) E. Casagrande, M. Back, D. Cristofori, J. Ueda, S. Tanabe, S. Palazzolo, F. Rizzolio, V. Canzonieri, E. Trave and P. Riello, *J. Mater. Chem. C*, **8**, 7828–7836 (2020).
13) M. Back, J. Ueda, H. Nabu, M. Fujita, A. Yamamoto, H. Yoshida, H. Tanaka, M. G. Brik and S. Tanabe, *Adv. Opt. Mater.*, **9**, 2100033 (2021).
14) M. Back, E. Trave, J. Ueda and S. Tanabe, *Chem. Mater.*, **28**, 8347–8356 (2016).
15) M. Back, J. Ueda, M. Brik and S. Tanabe, *ACS Appl. Mater. Inter.*, **12**, 38325–38332 (2020).
16) A. Benayas, B. del Rosal, A. Perez-Delgado, K. Santacruz-Gomez, D. Jaque, G. A. Hirata and F. Vetrone, *Adv. Opt. Mater.*, **3**, 687–694 (2015).
17) A. Skripka, A. Morinvil, M. Matulionyte, T. Cheng and F. Vetrone, *Nanoscale*, **11**, 11322–11330 (2019).
18) S. Balabhadra, M. L. Debasu, C. D. S. Brites, L. A. O. Nunes, O. L. Malta, J. Rocha, M. Bettinelli and L. D. Carlos, *Nanoscale*, **7**, 17261–17267 (2015).
19) P. M. Gschwend, F. H. L. Starsich, R. C. Keitel and S. E. Pratsinis, *Chem. Commun.*, **55**, 7147–7150 (2019).
20) R. G. Geitenbeek, A.-E. Nieuwelink, T. S. Jacobs, B. B. V. Salzmann, J. Goetze, A. Meijerink and B. M. Weckhuysen, *ACS Catal.*, **8**, 2397–2401 (2018).
21) T. Hartman, R. G. Geitenbeek, G. T. Whiting and B. M. Weckhuysen, *Nat. Catal.*, **2**, 986–996 (2019).
22) R. G. Geitenbeek, J. C. Vollenbroek, H. M. H. Weijgertze, C. B. M. Tregouet, A.-E. Nieuwelink, C. L. Kennedy, B. M. Weckhuysen, D. Lohse, A. van Blaaderen, A. van der Berg, M. Odijk and A. Meijerink, *Lab Chip*, **19**, 1236–1246 (2019).
23) T. P. van Swieten, T. van Omme, D. J. van den Heuvel, S. J. W. Vonk, R. G. Spruit, F. Meirer, H. H. Perez Garz, B. M. Weckhuysen, A. Meijerink, F. T. Rabouw and R. G. Geitenbeek, *ACS Appl. Nano Mater.*, **4**, 4208–4215 (2021).
24) J. Ueda and S. Tanabe, *Opt. Mater. X*, **1**, 100018 (2019).
25) J. Xu and S. Tanabe, *J. Lumin.*, **205**, 581–620 (2019).
26) J. E. Geusic, H. M. Marcos and L. G. Van Uitert, *Appl. Phys. Lett.*, **4**, 182 (1964).